

Biophysical Characterization of a Soluble CD40 Ligand (CD154) Coiled-Coil Trimer: Evidence of a Reversible Acid-Denatured Molten Globule

James E. Matsuura,^{*,1} Arvia E. Morris,[†] Randal R. Ketchum,[‡] Emory H. Braswell,[§] Ralph Klinke,[¶] Wayne R. Gombotz,^{*} and Richard L. Remmele, Jr.^{*,2}

^{*}Analytical Chemistry and Formulation, [†]Cell Sciences, [‡]Bioinformatics, and [¶]Product Recovery, Immunex Corporation, 51 University Street, Seattle, Washington 98101; and [§]Molecular & Cell Biology, University of Connecticut, U-125, Storrs, Connecticut 06269-3125

Received April 5, 2001; published online July 17, 2001

The CD40 ligand molecule is unique, consisting of a receptor-binding domain anchored by an isoleucine zipper moiety. Exact determination of the multimeric state and its tendency to form molten globules has not been elucidated. Corroborating evidence of a trimerized molecule in aqueous solution was obtained from size-exclusion chromatography, laser light scattering, and analytical ultracentrifugation. A reversible acid-denatured molten globule state was observed from circular dichroism and fluorescence spectroscopy data. The molten globule state was characterized by a loss of tertiary structure with associated retention of secondary structure near pH 3. Once returned to pH 7, the acid-denatured state refolded over the course of 7 days resulting in approximately 90% recovery of the native structure. The molten globule state was characterized by a broadening of structural features in the second-derivative spectra of Fourier transform infrared spectroscopy. A component band at 1650 cm⁻¹ was shown to be α -helix and originate from amide carbonyl vibrations of the isoleucine zipper. Differential scanning calorimetry measurements characterized the pH-sensitive molten globule state at pH 3.3 as one lacking a well-defined unfolding transition with an accompanying baseline shift at 58°C (a consequence of increased heat capacity). The tendency to form molten globules during acid denaturation stress permits an opportunity to study the process of partial protein unfolding with implications concerning stability. Although reversible molten globules can be formed, it is important

to recognize the unusual nature since the molten globule state is formed exclusively within the β -sheet receptor-binding region. © 2001 Academic Press

Key Words: CD40 ligand; coiled-coil; circular dichroism; Fourier transform infrared spectroscopy (FTIR); fluorescence; light scattering; analytical ultracentrifugation; microcalorimetry; molten globule; β -sheet.

CD40 ligand (CD40L) is a glycoprotein transiently expressed on activated T cells. It is required for isotype switching and maturation of B cells (1, 2) and plays a key role in additional immune responses (3). One of the more interesting aspects of CD40L concerns the relationship of multimericity and activity. The active form of CD40L is trimeric based on molecular modeling and X-ray crystallographic evidence of the CD40 binding region (4–6) and a study indicating trimer formation of the tumor necrosis factor (TNF)³ homologous portion of CD40L (7). Moreover, the addition of an isoleucine zipper motif to the amino terminus enhances the biological activity of soluble CD40L (2, 6). The isoleucine zipper motif was derived from GCN4 peptide which has been shown to form coiled-coil dimer, trimer, or tetramer structures depending on the amino acids substituted in positions 1 and 4 of the heptad repeat (8, 9). A trimer is expected if the 1 and 4 positions are all substituted with isoleucines. In addition, substitution of tryptophan (W) for cysteine (C) at amino

¹ Current address: Alza Corporation, 1501 California Avenue, Palo Alto, CA 94304.

² To whom correspondence and reprint requests should be addressed. Fax: 206-621-6952. E-mail: remmeler@immunex.com.

³ Abbreviations used: AUC, analytical ultracentrifugation; MW, molecular weight; DSC, differential scanning calorimetry; FTIR, Fourier transform infrared spectroscopy; SEC, size-exclusion chromatography; TNF, tumor necrosis factor; CHO, Chinese hamster ovary.

acid position 194 of the soluble CD40L molecule increases the binding of CD40L to its receptor (U.S. Patent No. 5,962,406). This coiled-coil isoleucine zipper version of the soluble CD40L (hereafter referred to as z-rhuCD40L) is a two-domain protein consisting of a predominantly β -sheet receptor-binding region containing the C to W substitution at position 194 and a putative helical coiled-coil isoleucine zipper motif to stabilize trimer formation (6, 10, 11).

Molten globules are compact denatured structures with near native secondary structure, significant loss of tertiary structure, and increased exposure of hydrophobic surface area (i.e., propensity to form aggregates) (12–14). There are a number of examples in the literature of partially folded intermediates involving α -helical proteins (12, 13, 15). However, there are only a few examples of molten globules involving β -sheet proteins (16–19). Molten globules of β -sheet proteins are difficult to produce because such a transition would require the retention of hydrogen bonding between β -strands while disrupting tertiary structure or the formation of isolated β -strands. It has been suggested that isolated β -strands are converted into α -helices which are more stable as single entities (20, 21). Thus, molten globules containing intact β -sheets are rare and require that tertiary structural mobility increase without significantly altering the contacts needed for β -sheet stabilization. The z-rhuCD40L binding domain, which is a β -sheet domain, will be shown to form a molten globule state, adding one more protein to the very short list of β -sheet molten globules.

MATERIALS AND METHODS

Expression of z-rhuCD40L in Chinese hamster ovary (CHO) cells. The soluble z-rhuCD40L molecule consists of an isoleucine zipper domain based upon a leucine zipper motif (8) at the N-terminus of the TNF homologous domain of the molecule (aa 113 to aa 261, Ref. 22). To enhance the activity and eliminate disulfide crosslinking of the soluble z-rhuCD40L, the sequence encoding the TNF-homologous extracellular portion of z-rhuCD40L was mutated at position 194 (tryptophan for cysteine, numbering system of Ref. 22). The hybrid construct consists of the trimerization domain and the mutein TNFr homologous region of CD40L. It was cloned 3' to the growth hormone leader sequence (23). The final z-rhuCD40L molecule included a ThrSerSerAsp peptide at the N-terminus and a LeuLeu at the junction between the trimerization motif and the TNFr homologous portion of the molecule as a result of cloning manipulations. The DNA fragment encoding z-rhuCD40L was subcloned into the mammalian expression vector 2A51 (24) using unique 5' *Xma*I and 3' *Not*I restriction sites for expression in CHO cells. Approximately 50% of the z-rhuCD40L molecules in a given sample are glycosylated at a single site.

Protein concentration. All concentrations were determined using an experimentally determined molar extinction coefficient, $\epsilon = 0.915$, at 280 nm [a theoretical value derived from primary sequence as described by Gill and Hippel (25) yielded a value of 0.918], which in turn was based on quantitative amino acid analysis.

Buffering systems. All buffer components were reagent grade or better obtained from sources listed below and used without further

purification. The polybuffer composition was chosen to minimize temperature-dependent pH changes during thermal unfolding experiments and to compensate for ionization effects during DSC measurements. It consisted of 50 mM sodium citrate (J. T. Baker), 20 mM sodium chloride (J. T. Baker), 20 mM sodium phosphate (Mallinckrodt), 17 mM L-arginine (EM Science), 40 mM glycine (J. T. Baker), 25 mM HEPES (Sigma), and 20 mM Hepes (J. T. Baker). A 1/10 dilution of the polybuffer containing 25% glycerol was used in the pH studies involving circular dichroism (CD), Fourier transform infrared spectroscopy (FTIR), and fluorescence measurements to minimize aggregation effects. Since higher concentrations were needed to evaluate the pH 3 sample in the FTIR data, 250 mM NaCl was added in that particular case. In the isoleucine zipper FTIR studies, Tris was used instead of polybuffer with 25% glycerol and 250 mM NaCl to avoid precipitation at 25 mg/ml.

Three-detector light scattering. Light-scattering measurements were performed with a DAWN multiangle laser-light-scattering instrument (MALLS; Wyatt Technology Corp.), in series with a refractive index detector (Optilab DSP; Wyatt Technology Corp.) and a UV detector (Integral HPLC from Perceptive Biosystems, Inc.). Molecular weights were determined using the three-detector method previously described (26–29). A calibration constant for all three detectors was determined using ribonuclease A, β -lactoglobulin, ovalbumin, bovine serum albumin monomer, and bovine serum albumin dimer. A plot of (LS) (UV)/ ϵ (RI)² (where LS is the light-scattering signal at 90°, UV is the absorbance at 280 nm, and RI is the signal from the refractive index detector) as a function of MW in each case yielded a straight line with a correlation coefficient, $r^2 = 0.993$. The signal obtained from the three detectors was evaluated in triplicate for all protein standards used in the calibration. Injections of 20 or 100 μ l of sample were eluted off a Pharmacia Superdex-200 size-exclusion column (Amersham Pharmacia Biotech) using a 0.5 ml/min flow rate. The elution buffer consisted of 200 mM sodium phosphate (pH 8) and was used for all dilutions of the samples. Samples ranged in concentration from 0.2 to 50 mg/ml.

Equilibrium analytical ultracentrifugation. The main peak was isolated and purified off of the Superdex-200 column and subjected to analytical ultracentrifugation studies (AUC). Sedimentation equilibrium experiments were carried out in a Beckman XL-I analytical ultracentrifuge (Beckman Instruments, Inc.). Protein samples were loaded at 0.5, 0.2, and 0.1 mg/ml into the solution channels of two six-channel cells (12-mm optical path) resulting in solution columns of 2.5 mm. The samples were spun at 17, 24, and 30 kRPM. Absorption optics (at 279 nm) were used to record the concentration gradient. Sedimentation equilibrium was determined to have been achieved when successive scans exhibited undetectable differences as measured by software ("MATCH" developed by D. Yphantis) that removes interfering effects such as rotor precession. Analysis was performed using a nonlinear least-squares program (30). Global fits were obtained by combining all data sets from different protein-loading concentrations and rotor speeds. The analysis proceeded by fitting the data from assumed models. Buoyant MW were corrected using a specific volume of 0.739 ml/g (calculated from amino acid sequence) and a solvent density of 1.0268 g/ml at 4°C.

CD. Circular dichroism data were determined on a Jasco J-600 spectropolarimeter. Temperature was controlled using a Neslab NTE-111 water bath ($\pm 0.1^\circ\text{C}$) with a remote sensor. Each CD spectrum represented a coverage of four consecutive scans using a 1-nm bandwidth, 1-nm step, and a 2-s averaging time. Quartz cuvettes ranging in pathlength from 0.01 mm to 1 cm were used to analyze samples consisting of a wide range of concentrations. Cuvette pathlengths and CD signal were checked using a standard camphor sulfonic acid solution (31). Spectra were corrected to mean residue ellipticity using a mean residue weight of 111.3. Convex-constraint analysis (CCA) (32) was used to deconvolute spectra into secondary structural components. The far-UV CD data were obtained using

protein concentrations of 0.1 mg/ml in a 1-mm-pathlength cuvette and the near-UV were taken at 1 mg/ml in a 1-cm cuvette.

Fluorescence spectroscopy. Fluorescence measurements were carried out using a SLM 8000 spectrofluorometer equipped with a temperature-controlled water bath (set at 20°C) and emission monochromator. All samples were diluted to 25 µg/ml in the appropriate buffer and excited at 295 nm with emission spectra collected from 300 to 400 nm in 1-cm quartz cuvettes.

FTIR. Fourier transform infrared spectra were collected using a Bio-Rad FTS-7 FTIR spectrometer. Solutions containing 38 mg/ml CD40L were examined in CaF₂ infrared cells with a 6-µm path-length. For each spectrum a 256-scan interferogram was collected in single-beam mode with a 4-cm⁻¹ resolution from 4000 to 1000 cm⁻¹. Spectra of these samples were evaluated by subtracting water vapor and buffer blank contributions in the region of the amide I band and then subsequently applying a Savitsky-Golay function to generate a second derivative of the absorbance spectrum (33). Secondary structural analysis was carried out by curve-fitting Fourier self-deconvoluted spectra (34, 35) in addition to inverted baseline-corrected second-derivative spectra (33).

Microcalorimetry. Differential scanning calorimetry data were acquired on a Microcal MC-2 (MicroCal, Inc.) with nominal protein concentrations of 3 mg/ml in polybuffer (developed to minimize pH variability with progressive heating and normalize solution component effects). Cleanliness of the DSC cells was checked by establishing reproducible water baseline runs prior to sample analysis to ensure the elimination of artifacts in a given run. The upscan rate was 68°C/h and all data were evaluated using the Origin software provided with the instrument.

Molecular modeling. The complete z-rhuCD40L:isoleucine trimer was modeled based on the Protein Data Bank (PDB) (36) entries 1gcm (residues 77–107) for the ILE zipper and 1aly (residues 116–261) for the ligand. Entry 1gcm contains the isoleucine zipper as a trimer and the biological unit of 1aly was used to represent the CD40L trimer. The linker region between the zipper and the ligand was modeled as helical up to residue 114, at which point the model merged with the coil structure defined by the N-terminus of 1aly. From this point the two cysteines known to form a disulfide bridge were covalently linked (residues 178–218) and the entire trimer was minimized with 100 steps of steepest descent followed by an unlimited number of steps of conjugate gradient to reach 0.1 kcal/Å. This produced the initial structure with a free cysteine at position 194. The free cysteine was replaced with tryptophan representing the sequence used in the biophysical studies. The side chain was replaced on each monomer and multiple rotamers were analyzed to obtain the lowest initial energy conformation. The entire molecule was once again minimized as before to allow for the propagation of structural changes induced by the introduction of the tryptophan residue. This produced the pH 7 structure.

RESULTS

Characterization of the Multimeric State of z-rhuCD40L Coiled-Coil

Light scattering. The three-detector light-scattering method has been used to determine the nonglycosylated MW of glycosylated proteins (26–29). The MW of the main peak eluting off of the size-exclusion column was determined to be approximately 60 kDa. It is noted that the MW measured by SEC was dependent upon the use of globular protein standards that assumes the unknown has a similar shape. Since z-rhuCD40L was presumed to have an unusual shape (possessing three receptor-binding globular domains

that are anchored to a coiled-coil isoleucine zipper and partially glycosylated), the MW needed to be verified by light scattering. The elution profile of the main peak for CD40L was analyzed using the three-detector method and found to be 61.3 ± 0.2 (very close to three times the monomer polypeptide MW of 20.34 kDa).

Equilibrium analytical ultracentrifugation. More data supporting the existence of a trimer in solution were obtained from AUC measurements. The data fit an ideal single-species model (RMS error of 0.009 AU) with little systematic error yielding a buoyant molecular weight [$M(1 - \bar{v} \rho)$] of 15.2 ± 0.8 kDa (95% confidence). Using the specific volume of the protein (assuming as a first approximation that the chain is only protein) and the density of the solvent, one obtains a Z-average MW of 63.0 ± 3.2 kDa (95% confidence) for the protein, clearly indicating its presence as a trimer. One can calculate the degree of glycosylation using the chain MW of the protein (from the amino acid composition), the specific volume of the protein (0.739 ml/g), the density of the solvent (1.0268 g/ml), an assumed value for the carbohydrate specific volume [0.65 ml/g (37)], and the experimentally determined value of the buoyant MW of the molecule. The result indicates that the average degree of glycosylation [1.5 ± 2.4 kDa (95% confidence) per trimer] is quite low. Upon adding this amount of glycosylation to the chain MW of the trimer, i.e., 61.0 kDa (3×20.34 kDa), one obtains for the total MW of the complex a value of 62.5 ± 2.4 kDa. This is not significantly different from that obtained by assuming that the molecule is all protein.

Unfolding/Refolding Studies

Circular dichroism studies on pH denaturation. Figure 1 shows the effect of pH on the structure of CD40L in 25% glycerol and polybuffer. The far-UV CD data show an increase in negative signal at wavelengths less than 220 nm with a concomitant decrease in negative signal near 222 nm comparing the spectrum at pH 7 to pH 3 (Fig. 1A). The differences displayed suggest a presumptive decrease in β -sheet with a small corresponding contribution to unordered structure at pH 3. Unfortunately, a quantitative assessment of the changes in secondary structure from pH 7 to pH 3 is difficult since the position and intensity of the positive band around 190 nm could not be collected due to limitations of instrumentation and buffer conditions (38, 39). While the secondary structure remains near native, the tertiary structure in the near-UV (Fig. 1B) indicates a significantly altered conformation showing conversion from a positive tryptophan band at pH 7 to a state that is predominated by a negative tyrosine signal at pH 3. This behavior is expected for a molten globule state.

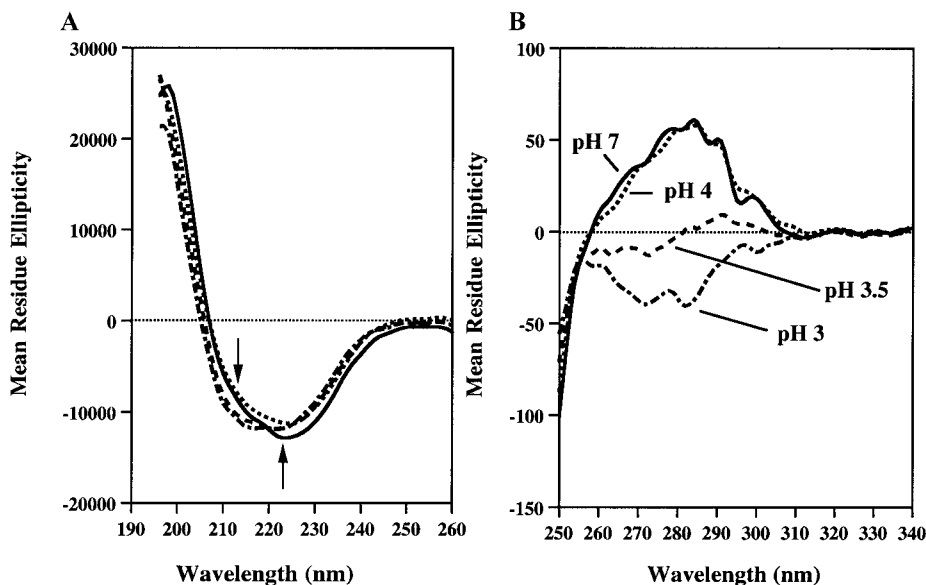


FIG. 1. The effect of pH on secondary and tertiary structure of z-rhuCD40L. The far-UV CD (A) and near-UV CD (B) at pH 7 (solid lines), pH 4.1 (dotted lines), pH 3.5 (dashed lines), and pH 2.9 (dot-dash lines). Arrows indicate directions of change.

It should be noted that unfolding experiments with guanidinium produced a cooperative transition with no apparent decoupling of the secondary and tertiary structure (data not shown). There was also no evidence for an intermediate state exhibiting a loss of tertiary structure and the retention of significant secondary structure.

Refolding experiments with samples of CD40L kept at pH 3 for 1 h and returned to pH 7 initially exhibited

no significant near-UV CD native structure. However, given enough time the protein did begin to refold from the acid-denatured state, albeit very slowly (Fig. 2). Although a native-like near-UV spectrum was observed after 7 days (Fig. 2B), a small fraction of incompletely refolded sample remained. Judging by the small difference in spectral intensity when compared to the native spectrum, it is quite possible that the incomplete refolding is the result of soluble aggregate

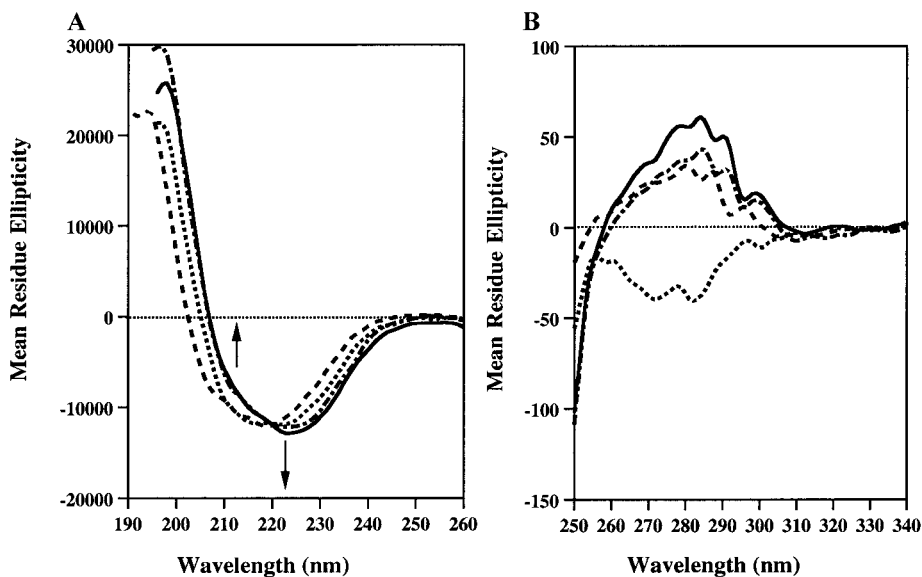


FIG. 2. Refolding of z-rhuCD40L from the acid denatured state. The far-UV CD (A) and the near-UV CD (B) of native protein at pH 7 (solid lines) and pH 3 (dotted lines). The samples are then readjusted to pH 7 and allowed to refold for 3 days (dashed lines) and 7 days (dot-dash lines). All samples are in a polybuffer, with 25% glycerol at 1 mg/ml. Far-UV CD spectra were collected using a 0.1-mm-pathlength cuvette. Arrows indicate directions of change.

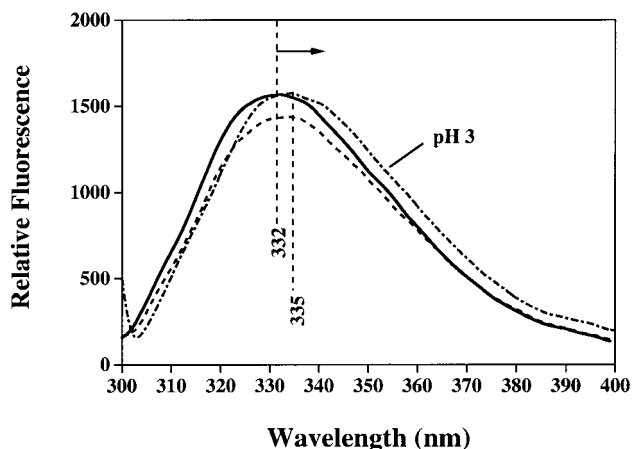


FIG. 3. Fluorescence spectra for z-rhuCD40L excited at 295 nm. Native protein is in polybuffer containing 25% glycerol at pH 7 (solid contour), pH 3 (dot-dash contour), and 7-day refold from pH 3 (dotted contour). All spectra collected were of 25 $\mu\text{g/ml}$ protein in 1-cm rectangular quartz cuvettes.

formation. Size-exclusion data showed an increase in aggregate formation comprising about 10% of the refolded samples (data not shown). This amount of aggregation can account for the decreased intensity of the near-UV CD spectrum and thus, the decrease in the refolded z-rhuCD40L is assumed to be due to soluble aggregates formed from a competing reaction with the molten globule state. Despite this observation, the shape and band positions of the near-UV spectra for the refolded z-rhuCD40L sample were found to be very similar to those of the native tertiary structure.

Fluorescence studies. The samples from the CD pH refolding studies were examined further by fluorescence spectroscopy. The fluorescence spectra (Fig. 3) for the native, acid-denatured (pH 3), and refolded protein tell a similar story. The acid-denatured sample exhibits a small red shift as shown by the arrow from the native maximum position in Fig. 3. Refolding at pH 7 exhibits a near-native structure with decreased signal intensity approximating that seen from the near-UV CD after 7 days (Fig. 2B). Again, the decreased amount of fluorescence could be attributed to aggregate formation (10% aggregate as indicated by size-exclusion chromatography measurements). The fluorescence data complement the CD results showing significant refolding from the acid-denatured state.

FTIR studies. Several studies in the literature have analyzed the amide I region of the infrared to verify intact secondary structure for the molten globule state (40, 41). In this study, further verification of retained secondary structure in the acid-induced molten globule is shown by second-derivative FTIR spectra (Fig. 4A). The spectra show no change in secondary structure at pH 7 in Tris or in polybuffer containing

25% glycerol. Additionally, there is little change in band position at pH 3 in polybuffer, 25% glycerol, and 250 mM NaCl. Based on the CD results, it was not surprising to see very little change in secondary structure at pH 3 by FTIR. The spectrum at pH 3 does show an increased bandwidth and some loss in peak resolution indicating a loosened structure. Overall peak positions and intensities are comparatively similar for all three second-derivative spectra.

FTIR and CD of the isoleucine zipper. A comparison of the second-derivative FTIR spectra of z-rhuCD40L and the 36-amino-acid coiled-coil peptide is shown in Fig. 4B. There are two main features that are different in the zipper spectrum from that of the z-rhuCD40L spectrum. The first is that there is an increased bandwidth of the zipper spectrum that could arise from differences in z-rhuCD40L concentration (35 mg/ml) compared to the zipper peptide (25 mg/ml). Alterna-

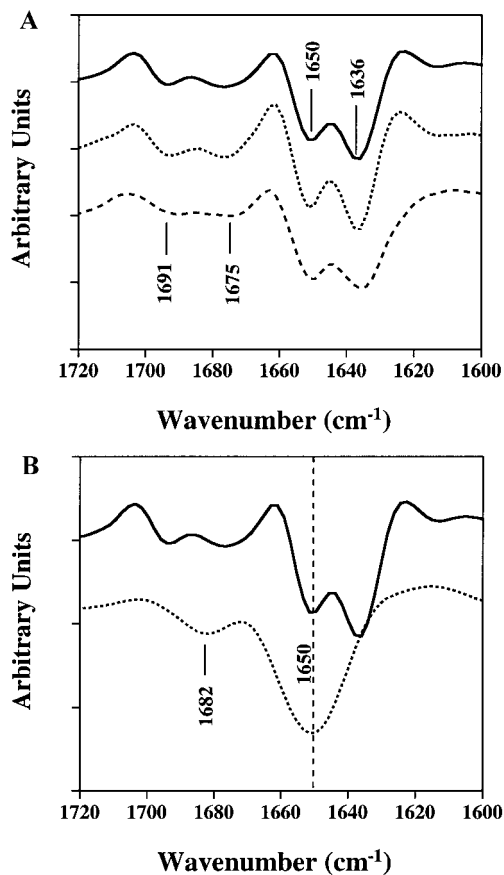


FIG. 4. Second-derivative FTIR spectra (A) of z-rhuCD40L in 50 mM Tris at pH 7 with no glycerol (solid contour), in 25% glycerol and polybuffer at pH 7 (dotted contour), and in 25% glycerol (and 250 mM salt) and polybuffer at pH 3 (dashed contour). (B) Second-derivative FTIR spectra of 38 mg/ml z-rhuCD40L (solid contour) and accompanying trimerized isoleucine zipper peptide (dotted contour) at 25 mg/ml; both samples were evaluated in 25% glycerol and 50 mM Tris at pH 7.

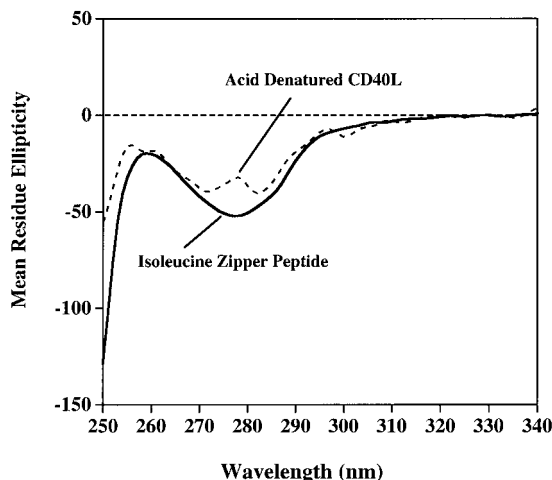


FIG. 5. The 20°C near-UV CD of the isoleucine zipper peptide at pH 7 (solid contour) and acid-denatured z-rhuCD40L at pH 3 (dashed contour). Note that the tertiary structural change of the protein contains a fine structure that is absent in the isoleucine zipper peptide.

tively, since the isoleucine zipper is a 36-amino-acid peptide, the band broadening may simply be due to a less rigid structure than that expected for the isoleucine zipper coiled-coil attached to the protein. The second feature is a main band signal of the zipper peptide that corresponds to the second most intense band of the z-rhuCD40L spectrum. The position of this band (at 1650 cm^{-1}) is usually assigned to an unordered structure (42, 43). However, since bands typically assigned to the α -helix occur near $1656 \pm 2\text{ cm}^{-1}$ and those for an unordered structure occur near $1648 \pm 2\text{ cm}^{-1}$, it has generally been difficult to resolve them and make an assignment based on FTIR frequency alone (44). Thus, evidence from a complementary technique was required to confirm the assignment. Such evidence was acquired from far-UV CD measurements.

The far-UV CD of the zipper peptide clearly demonstrated an α -helical spectrum, with very little contribution from other secondary structures. Based on the mean residue molar ellipticity signal at 222 at 20°C ($-31,742$), there is about 97% α -helix (45).

The near-UV CD of the isoleucine coiled-coil is shown in Fig. 5. Although the tyrosine in this peptide is not expected to be CD active due to solvent exposure, a similar spectrum was reported for the GCN4 leucine zipper dimer (46). Interestingly, the structure of the z-rhuCD40L spectrum at pH 3 indicates a similar resemblance to that seen for the isoleucine zipper peptide at pH 7, except that it contains some tryptophan and tyrosine fine structure. Even though there is one tyrosine in the zipper, its contribution to the residual tertiary structure of the molten globule is expected to be small in comparison to those of the receptor-binding domain. This is borne out by the fact that the receptor-

binding domain contains five residues of tyrosine and two residues of tryptophan and also since in Fig. 5 the isoleucine zipper is devoid of fine structure that is clearly present in the z-rhuCD40L molecule. Furthermore, because all tryptophans and the majority of tyrosines are localized in the receptor-binding domain, the greatest contributions to the changes observed in the near-UV fine structure of the z-rhuCD40L molecule at pH 3 are consistent with tertiary structure alterations involving primarily the receptor-binding domain.

DSC studies. Concentration-normalized thermal denaturation traces of CD40L at different pH values are shown in Fig. 6. The highest melting temperatures were observed for the scans at pH 6.3 and pH 7.5. Hence, it follows that the greatest conformational stability is achieved within this pH range. In addition to the endothermic unfolding of the molecule, progressive heating beyond the transition resulted in a relatively sharp exothermic transition in each case. This feature is associated with protein precipitation. Approaching low or high pH conditions causes a decrease in the endothermic melting temperature accompanied by transition broadening. Finally, at pH 3.3 there was an absence of the endothermic transition and an unexplained baseline shift (as shown by the arrow in Fig. 6) was also found to be a characteristic feature in the DSC of yeast-derived z-rhuCD40L near pH 3.9 (data not shown for yeast z-rhuCD40L).

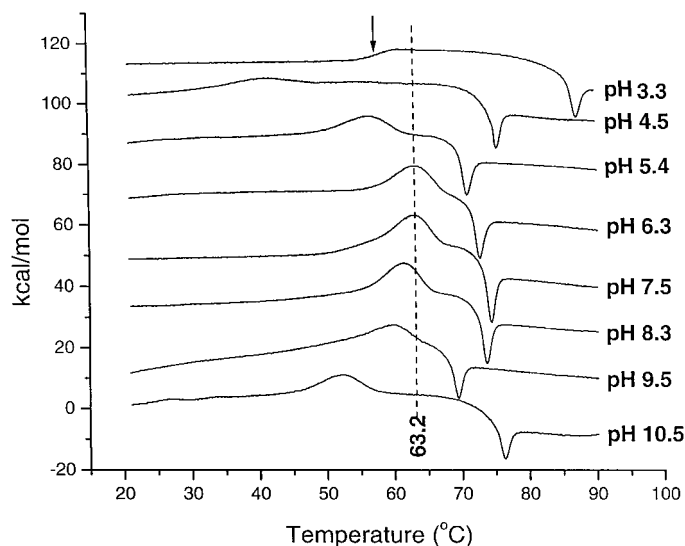


FIG. 6. DSC scans of z-rhuCD40L at 3 mg/ml in polybuffer at the indicated pH values. The highest melting transition is seen at 63.2°C. Note the endothermic baseline shift that occurs between 55 and 60°C at pH 3.3 (shown by arrow). The exothermic spike that follows the unfolding transition is characteristic of aggregation.

DISCUSSION

The intent and primary focus of this study were to characterize the multimeric state and physical properties associated with pH-induced unfolding of z-rhuCD40L. Molten globule formation during acid denaturation stress can provide insight about the physical nature of partially folded intermediates and their relationship to stability. In this case it was important to define the partially folded state of the molecule at pH 3.

Although there was some biological evidence that soluble versions of z-rhuCD40L formed a trimer, physical evidence of the multimeric state of z-rhuCD40L had not been fully elucidated (2). Knowing that the isoleucine zipper version of z-rhuCD40L could be unusual in size and shape, it was important to use credible techniques for accurate MW determination. The assessment of MW using SEC alone was subject to error given the dependence on elution time and possible column matrix interactions that can vary significantly with protein size and shape. There are examples of proteins whose MW determined by SEC have been inaccurate and shown only to be correctly determined by AUC (47) or light scattering (28, 29). Light scattering and AUC were therefore the preferred methods to accurately measure the MW and determine with a high level of certainty the multimerized form of z-rhuCD40L.

The monomer MW of z-rhuCD40L is 20.34 kDa based on the primary sequence. The MW of z-rhuCD40L determined by the three-detector light-scattering method was 61.3 kDa. This result supported a trimerized coiled-coil z-rhuCD40L molecule. Further evidence was acquired from AUC studies that revealed a MW of 63.0 kDa using a single species model. Both resulted in MW consistent with a 63-kDa trimer. The differences seen between the two MW are consistent with the degree of glycosylation for z-rhuCD40L. The three-detector technique exclusively evaluated the MW of the polypeptide chain, while the AUC measurement determined the MW of the entire ensemble. These results agreed with the SEC assessment and suggested that the multimeric form of the molecule in solution was indeed trimeric. The comparative agreement between the SEC and light-scattering data would indicate that the shape characteristics of the molecule are not so unusual after all. That is to say that the coiled-coil domain and glycosylation do not significantly alter the Stokes radius of the molecule enough to cause a deviation in elution time that is different from that expected using the globular protein standards. These data are similar to findings with other coiled-coil versions of z-rhuCD40L which do not have the cysteine to tryptophan substitution at amino acid position 194 (6).

The native z-rhuCD40L receptor-binding domain is predominantly β -sheet as determined by structural studies (48, 49) and exhibited by CD measurements of the receptor-binding domain. Contributions from α -he-

lix are primarily due to the coiled-coil isoleucine zipper. This being the case, it is emphasized that there are two tryptophans in z-rhuCD40L, both of which are in the β -sheet receptor-binding domain. Since the only two tryptophans in this molecule are located in this domain, it must mean that changes in the near-UV CD originate from a loss of tertiary structure in this domain with little consequence involving the coiled-coil. Thus, two criteria for a molten globule state are satisfied with these data, namely, a loss of tertiary structure and retention of near native secondary structure that can be envisioned to involve primarily the receptor-binding domain of the molecule. It must be noted that there were no visible signs of precipitation for the samples studied by CD. However, SEC indicated a propensity to aggregate where about 10% of the z-rhuCD40L were shown to form higher MW aggregates. Moreover, additional SEC experiments were conducted that showed that the trimer remained intact at pH 3. The greater extent at which aggregates formed at pH 3 satisfied a third characteristic of molten globules. The only aromatic group in the isoleucine coiled-coil is a single tyrosine. Molten globules are commonly found for proteins under mild denaturing conditions, producing intermediates with significant secondary structure and loss of tertiary structure. Formation of the molten globule was even more interesting given that the tertiary structure loss was localized to the β -sheet receptor-binding domain.

Secondary Structural Analysis

The secondary structure of native z-rhuCD40L was shown to consist primarily of α -helix and β -sheet by CD and FTIR measurements. Although the predominant FTIR frequency of the isoleucine zipper moiety was shown to occur where random structure contributions would be expected (near 1650 cm^{-1}), the far-UV CD measurements clearly confirmed that it was primarily α -helix. Curve fitting of the amide I band of z-rhuCD40L resulted in about 46% β -sheet and 30% α -helix/random coil. Since in these studies the FTIR bands for random coil and α -helix in the amide I were not separable, concise determination of the helix content was not possible by FTIR. With this in mind and building on evidence previously established, most of the α -helix content was attributed to the coiled-coil and that of the β -sheet to the receptor-binding domain.

Spectral deconvolution using convex-constraint analysis of the far-UV CD resulted in about 41% β -sheet and 24% α -helix at pH 7 representing native structure. This estimate is similar to that obtained from the FTIR measurements. At pH 3, the β -sheet content was found to decrease to approximately 26% and the α -helix remained essentially unchanged (about 24%). In addition, difference spectra (far-UV CD at pH

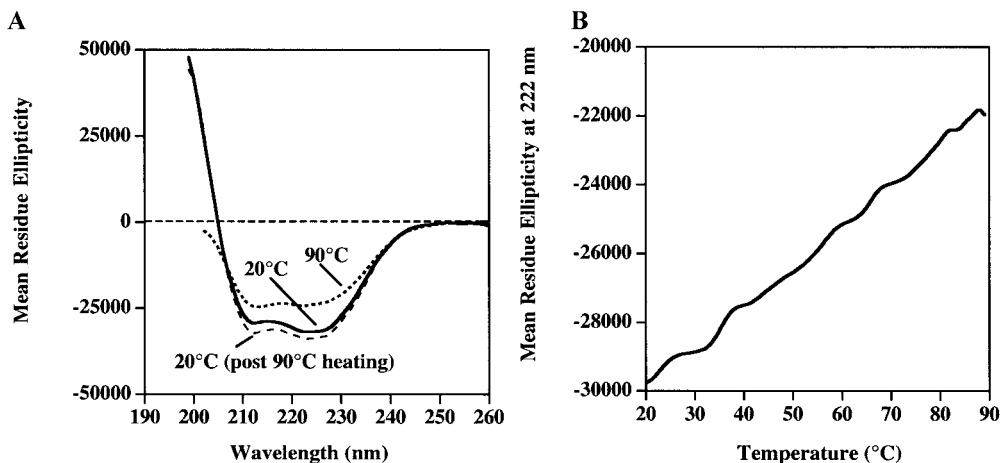


FIG. 7. The far-UV CD of (A) the isoleucine zipper peptide at 20°C (solid contour), thermally denatured at 90°C (dotted contour), and returned to 20°C after heating (dashed contour). Note that the postheated sample exhibits little evidence of structural change (thermally reversible), but does indicate that thermal denaturation significantly alters the secondary structure of the peptide. (B) The thermal unfolding behavior of the peptide is not a cooperative unfolding event as measured at 222 nm with progressive heating of the sample at pH 7 in 25 mM Tris, 25% glycerol, and 250 mM NaCl.

7 minus pH 3) indicate a loss of β -sheet (data not shown). These findings imply that the molten globule state of the protein involves little change in the coiled-coil and support small changes in secondary structure constituting a reduction in the β -sheet content of the receptor-binding domain. Acid denaturation is believed to form molten globules due to charge repulsion below the pK_a of the acidic groups (50, 51).

The reversibility of the acid-denatured state implies thermodynamic control of the molten globule form of the z-rhuCD40L molecule. It is interesting to note that approximately 90% of the refolded molecule is recovered when the pH is adjusted from 3 to 7. These results suggest that relatively small structural changes in the z-rhuCD40L molecule are prone to form soluble aggregates and indicate that the molten globule state (governed by the equilibrium between the native and partially folded state) is rate limiting with regard to aggregate formation.

Since lowering the pH to 3 forms the molten globule, DSC studies were used to monitor the enthalpic transitions at various pH values (Fig. 6). At pH 7 the enthalpic transition was characterized by the highest thermal stability with a melting temperature near 63°C. However, as pH was lowered toward 3, which is where the acid-induced molten globule is formed, there was a progressive loss of transition enthalpy and a continued shift toward lower melting transition temperatures. This is not unexpected for a protein whose thermally denatured state is the molten globule (12, 52). Second consecutive up-scans were also attempted at each pH condition and shown to exhibit no thermal reversibility.

In contrast to the irreversible nature of the z-rhuCD40L molecule, Fig. 7 shows the affects of heat-

ing the isoleucine zipper (pH 7) from 20 to 90°C and then back to 20°C. No evidence for cooperative unfolding was observed (Fig. 7B). However, changes in secondary structure that indicated a 25% loss in helix content based on the signal at 222 nm (45) were completely reversible upon return to 20°C (Fig. 7A). Such thermal reversibility behavior concerning leucine zippers is not an uncommon occurrence (53).

The absence of thermal reversibility at any pH tested for z-rhuCD40L in Fig. 6 is consistent with the receptor-binding domain being primarily responsible for the formation of aggregate and that it occurs involving a partially folded (molten globule-like) intermediate state exhibiting a small change in structure. Moreover, the wild type (without the isoleucine zipper) is prone to aggregation during DSC heating and irreversibly denatures in contrast to the isoleucine zipper behavior (6). The role of the isoleucine zipper has been shown to contribute to thermostability in the same DSC studies comparing wild-type rhuCD40L (without isoleucine zipper) to the same with the isoleucine zipper exhibiting a 10°C increase in melting transition temperature (6).

The lack of a well-defined enthalpic transition at pH 3 implies a molten globule where the receptor-binding domain has reached a partially unfolded state (or loosened structure). Unexpected in the results was the occurrence of a measurable endothermic baseline shift upon thermal heating (shown by the arrow near 58°C in Fig. 6). The assignment of the baseline shift has not been identified, but might be associated with an increased penetration of solvent into buried (hydrophobic) regions of the molecule. Hence, the endothermic baseline shift may originate from a thermal transition that involves penetration and perhaps partial dissoci-

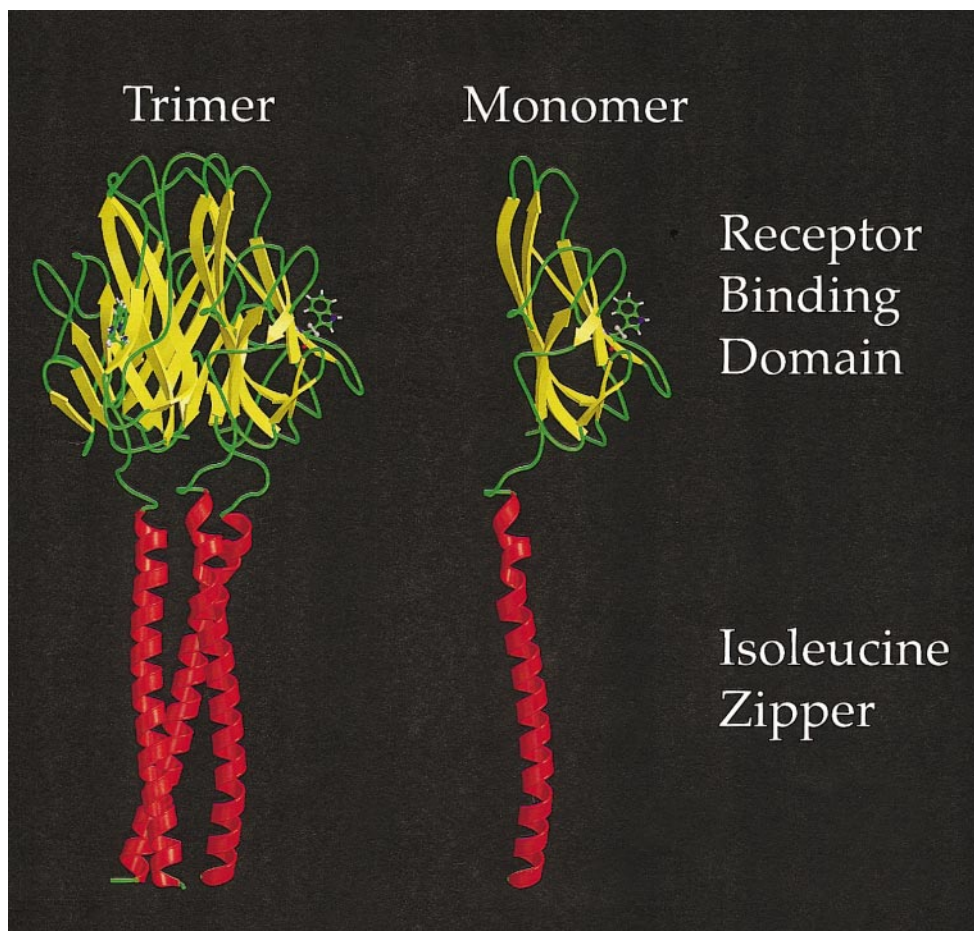


FIG. 8. Molecular model showing the receptor-binding domain and isoleucine zipper domains in a trimer and monomer arrangement at pH 7. The mutated tryptophan (194 position) is shown as a ball and stick representation on the receptor-binding domain.

ation of the isoleucine zipper coils at elevated temperatures near 58°C that would expose more hydrophobic surface area to the solvent (54).

Figure 8 is a visual assessment showing a three-dimensional model of the z-rhuCD40L molecule as a trimer and monomer. The secondary structure of the two domains is shown to be different given the helix content that is exclusively a part of the coiled-coil region and the sheet region exclusively found in the receptor-binding domain. Biophysical evidence has been presented that establishes z-rhuCD40L as a trimer in solution. It has also been shown that a reversible molten globule state is attained at pH 3. The molten globule is a partially folded intermediate state that is susceptible to form aggregated products facilitated by a structural alteration in the receptor-binding domain of this molecule.

CONCLUSIONS

The z-rhuCD40L molecule exists as a coiled-coil trimer in solution as determined by light scattering

(three-detector method), AUC, and SEC. Evidence has been presented for a molten globule state that exhibited little change in secondary structure (corroborated by infrared and far-UV CD) with corresponding major changes in tertiary structure as measured by near-UV CD. Acid denaturation of the molecule near pH 3 is nearly 90% reversible upon renaturation at pH 7 over a 7-day period. The evidence presented meets the criteria for a molten globule exhibiting little loss in secondary structure with major tertiary structure changes and a propensity to form aggregates. Moreover, the molten globule state is an intermediate state between the native and fully extended denatured state.

Evidence presented from secondary structure assessments of the far-UV CD suggests that the receptor-binding domain of the molecule and not the isoleucine zipper moiety is most responsible for the molten globule state. This has been supported by the fact that the molten globule state at pH 3 exhibits a small loss of β -sheet that is exclusively associated with the receptor-binding domain. Second, the α -helix content at pH

3 remains essentially unchanged suggesting that the coiled-coil domain is intact (also supported by SEC light-scattering data). Third, alterations associated with tertiary structure are consistent with changes primarily involving tryptophan residues located exclusively in the receptor-binding domain. Fourth, examination of the isoleucine zipper in the near-UV CD region is devoid of fine structure, indicating that most if not all of the tertiary structure is altered in the receptor-binding domain. The information presented not only enhances one's understanding of the destabilizing forces associated with a partially folded state, but further elucidates the influences that small structural changes can have originating from primarily β -sheet regions of the molecule.

REFERENCES

1. Spriggs, M. K. (1994) in *Mechanisms of Lymphocyte Activation and Immune Regulation V* (Gupta, S., Ed.), pp. 239–244, Plenum Press, New York.
2. Fanslow, W. C., Srinivasan, S., Paxton, R., Gibson, M. G., Spriggs, M. K., and Armitage, R. J. (1994) *Semin. Immunol.* **6**, 267–278.
3. Grewal, I. S., and Flavell, R. A. (1997) *Immunol. Res.* **16**, 59–70.
4. Bajorath, J., Stenkamp, R., and Aruffo, A. (1993) *Protein Sci.* **2**, 1798–1810.
5. Aruffo, A., Farrington, M., Hollenbaugh, D., Li, X., Milatovich, A., Nonoyama, S., Bajorath, J., Grosmaire, L. S., Stenkamp, R., Neubauer, M., Roberts, R. L., Noelle, R. J., Ledbetter, J. A., Francke, U., and Ochs, H. D. (1993) *Cell* **72**, 291–300.
6. Morris, A. E., Remmele, R. L., Jr., Klinke, R., Macduff, B. M., Fanslow, W. C., and Armitage, R. J. (1999) *J. Biol. Chem.* **274**, 418–423.
7. Mazzei, G. J., Edgerton, M. D., Losberger, C., Lecoanet-Henchoz, S., Graber, P., Durandy, A., Gauchat, J. F., Bernard, A., Allet, B., and Bonnefoy, J. Y. (1995) *J. Biol. Chem.* **270**, 7025–7028.
8. Harbury, P. B., Zhang, T., Kim, P. S., and Alber, T. (1993) *Science* **262**, 1401–1407.
9. DeLano, W. L., and Brunger, A. T. (1994) *Proteins* **20**, 105–123.
10. Harbury, P. B., Kim, P. S., and Alber, T. (1994) *Nature* **371**, 80–83.
11. Woolfson, D. N., and Alber, T. (1995) *Protein Sci.* **4**, 1596–1607.
12. Ptitsyn, O. B. (1995) *Adv. Protein Chem.* **47**, 83–229.
13. Fink, A. L. (1995) *Annu. Rev. Biophys. Biomol. Struct.* **24**, 495–522.
14. Dobson, C. M. (1994) *Curr. Biol.* **4**, 636–640.
15. Haynie, D. T., and Freire, E. (1993) *Proteins* **16**, 115–140.
16. Barbar, E., Barany, G., and Woodward, C. (1995) *Biochemistry* **34**, 1142–1134.
17. Kumar, T. K., Jayaraman, G., Lee, C. S., Sivaraman, T., Lin, W. Y., and Yu, C. (1995) *Biochem. Biophys. Res. Commun.* **207**, 536–543.
18. Sivaraman, T., Kumar, T. K., Jayaraman, G., Han, C. C., and Yu, C. (1997) *Biochem. J.* **321**, 457–464.
19. Dalessio, P. M., and Ropson, I. J. (1998) *Arch. Biochem. Biophys.* **359**, 199–208.
20. Liu, Z. P., Rizo, J., and Gierasch, L. M. (1994) *Biochemistry* **33**, 134–142.
21. Narhi, L. O., Philo, J. S., Li, T., Zhang, M., Samal, B., and Arakawa, T. (1996) *Biochemistry* **35**, 11454–11460.
22. Spriggs, M. K., Armitage, R. J., Strockbine, L., Clifford, K. N., Macduff, B. M., Sato, T. A., Maliszewski, C. R., and Fanslow, W. C. (1992) *J. Exp. Med.* **176**, 1543–1550.
23. Pecceu, F., Dousset, P., Shire, D., Cavois, E., Marchese, E., Ferrara, P., Kaghad, M., Dumont, X., and Lupker, J. (1991) *Gene* **97**, 253–258.
24. Morris, A. E., Lee, C. C., Hodges, K., Aldrich, T. L., Krantz, C., Smidt, P. S., and Thomas, J. N. (1997) in *Animal Cell Technology* (Carrondo, M. J. T., Griffiths, B., and Moreira, J. L. P., Eds.), pp. 529–534, Kluwer Academic, The Netherlands.
25. Gill, S. C., and von Hippel, P. H. (1989) *Anal. Biochem.* **182**, 319–326.
26. Arakawa, T., Langley, K. E., Kameyama, K., and Takagi, T. (1992) *Anal. Biochem.* **203**, 53–57.
27. Arakawa, T., Wen, J., and Philo, J. S. (1994) *Arch. Biochem. Biophys.* **308**, 267–273.
28. Wen, J., Arakawa, T., Talvenheimo, J., Welcher, A. A., Horan, T., Kita, Y., Tseng, J., Nicolson, M., and Philo, J. S. (1996) in *Techniques in Protein Chemistry VII* (Marshak, D. R., Ed.), Academic Press, New York.
29. Wen, J., Arakawa, T., and Philo, J. S. (1996) *Anal. Biochem.* **240**, 155–166.
30. Johnson, M. L., Correia, J. J., Yphantis, D. A., and Halvorson, H. R. (1981) *Biophys. J.* **36**, 575–588.
31. Cassim, J. Y., and Yang, J. T. (1969) *Biochemistry* **8**, 1947–1951.
32. Perczel, A., Hollosi, M., Tusnady, G., and Fasman, G. D. (1991) *Protein Eng.* **4**, 669–679.
33. Dong, A., Huang, P., and Caughey, W. S. (1990) *Biochemistry* **29**, 3303–3308.
34. Surewicz, W. K., and Mantsch, H. H. (1988) *Biochim. Biophys. Acta* **952**, 115–130.
35. Byler, D. M., and Susi, H. (1986) *Biopolymers* **25**, 469–487.
36. Berman, H. M., Westbrook, J., Feng, Z., Gilliland, G., Bhat, T. N., Weissig, H., Shindyalov, I. N., and Bourne, P. E. (2000) *Nucleic Acids Res.* **28**, 235–242.
37. Durchslag, H. (1986) in *Thermodynamic Data for Biochemistry and Biotechnology* (Hinz, H.-J., Ed.), pp. 45–116, Springer Verlag, Berlin.
38. Johnson, W. C., Jr. (1990) *Proteins* **7**, 205–214.
39. Bloemendal, M., and Johnson, W. C., Jr. (1995) in *Physical Methods to Characterize Pharmaceutical Proteins* (Herron, J. N., Ed.), Plenum Press, New York.
40. Yamasaki, K., Taniguchi, Y., Takeda, N., Nakano, K., Yamasaki, T., Kanaya, S., and Oobatake, M. (1998) *Biochemistry* **37**, 18001–18009.
41. Sosnick, T. R., and Trewheella, J. (1992) *Biochemistry* **31**, 8329–8335.
42. Dong, A., and Caughey, W. S. (1994) *Methods Enzymol.* **232**, 139–175.
43. Arrondo, J. L., Muga, A., Castresana, J., and Goni, F. M. (1993) *Prog. Biophys. Mol. Biol.* **59**, 23–56.
44. Azpiazu, I., and Chapman, D. (1992) *Biochim. Biophys. Acta* **1119**, 268–274.
45. Che, Y.-H., Yang, J. T., and Martinez, H. M. (1972) *Biochemistry* **11**, 4120–4131.

46. Holtzer, M. E., Adams, K., Lovett, E. G., and Holtzer, A. (1996) *Biopolymers* **38**, 669–671.
47. Shire, S. J. (1994) in *Modern Analytical Ultracentrifugation: Acquisition and Interpretation of Data for Biological and Synthetic Polymer Systems* (Schuster, T. M., and Laue, T. M., Eds.), Birkhauser Boston, Cambridge, MA.
48. Karpusas, M., Hsu, Y. M., Wang, J. H., Thompson, J., Lederman, S., Chess, L., and Thomas, D. (1995) *Structure* **3**, 1031–1039.
49. Peitsch, M. C., and Jongeneel, C. V. (1993) *Int. Immunol.* **5**, 233–238.
50. Goto, Y., Takahashi, N., and Fink, A. (1972) *Biochemistry* **29**, 3480–3488.
51. Fink, A. L., Calciano, L. J., Goto, Y., Kurotsu, T., and Palleros, D. R. (1994) *Biochemistry* **33**, 12504–12511.
52. Kuwajima, K. (1989) *Proteins* **6**, 87–103.
53. Holtzer, M. E., Lovett, E. G., d'Avingnon, D. A., and Holtzer, A. (1997) *Biophys. J.* **73**, 1031–1041.
54. Livingstone, J. R., Spolar, R. S., and Record, M. T., Jr. (1991) *Biochemistry* **30**, 4237–4244.